forests

MDPI

Article

Seasonal Growth of Pine Tree Rings: Comparison of Direct Observations and Simulation

Elena A. Babushkina [1], Gleb A. Sitnikov [1], Keshav K. Upadhyay [2], Dina F. Zhirnova [1], Grigory K. Zelenov [3], Eugene A. Vaganov [3,4] and Liliana V. Belokopytova [1,*]

[1] Khakass Technical Institute, Siberian Federal University, 655017 Abakan, Russia
[2] Department of Forestry, Mizoram University, Aizwal 796004, India
[3] Institute of Ecology and Geography, Siberian Federal University, 660041 Krasnoyarsk, Russia
[4] Department of Dendroecology, V.N. Sukachev Institute of Forest, Siberian Branch of the Russian Academy of Science, 660036 Krasnoyarsk, Russia
* Correspondence: white_lili@mail.ru

Abstract: Repetitive observations (direct measurements) of seasonal kinetics of xylogenesis and simulations (proxy data) with tree growth models are the two main approaches available to assess tree-ring growth and development. Both have drawbacks: short cover period for observations; limited accuracy of simulations depending on input data for models. We proposed an implementation of both approaches on the same trees to find ways for compensation. Cell numbers at subsequent xylogenesis stages were observed for *Pinus sylvestris* L. over five seasons in moisture-deficient habitats of Southern Siberia. The Vaganov–Shashkin model was parameterized for species and soil-landscape conditions to fit local tree-ring width chronologies (R = 0.56–0.73). Seasonal kinetics variables were then compared among themselves and with the simulated environmentally driven growth rate. The number of cells in the cambial and cell enlargement zone closely followed the curve of the 15-day moving average of the simulated growth rate (R = 0.56–0.87 at one site and R = 0.78–0.89 after shifting rate curve forward by 17–20 days at another site). The maximum number of cambium cells, which occurred within three weeks of the summer solstice, was found to be positively related with the number of tracheids in the complete tree ring (R^2 = 0.12–0.75 for individual seasons and 0.49 for total dataset), making it a promising short-term forecast variable for tree radial growth and productivity.

Keywords: continental Siberia; drought-sensitive habitat; *Pinus sylvestris* L.; tree rings; seasonal growth kinetics; xylogenesis; cambium cells; cells in enlargement zone; tree growth modeling; Vaganov–Shashkin process-based model

Citation: Babushkina, E.A.; Sitnikov, G.A.; Upadhyay, K.K.; Zhirnova, D.F.; Zelenov, G.K.; Vaganov, E.A.; Belokopytova, L.V. Seasonal Growth of Pine Tree Rings: Comparison of Direct Observations and Simulation. *Forests* **2022**, *13*, 1978. https://doi.org/10.3390/f13121978

Academic Editors: Giovanni Leonelli and Giacomo Alessandro Gerosa

Received: 29 September 2022
Accepted: 21 November 2022
Published: 23 November 2022

1. Introduction

Modeling is an effective tool for analyzing plant growth and development processes, which helps overcome the costs and commitment required from individuals and organizations in long-term forest monitoring [1–4]. It is notably useful in comprehending the complex reactions of temporal and spatial patterns in forest structure and function to a changing environment, but experimental verification of model algorithms is often limited or extremely difficult [5,6]. The developed models of the seasonal growth of xylem face limitations from the short duration of direct observations and/or the complexity of measuring the seasonal dynamics of cellular and especially cytoplasmic components [7–10]. Therefore, it has not yet been possible to directly test many promising hypotheses, such as spatial control of cambium functioning by the balance of major hormones [11–17]. More circumstantial evidence is used in these cases, such as testing if models based on these hypotheses conform to available observations of seasonal growth kinetics and/or wood anatomical structure.

Coniferous wood predominantly consists of regular radial files of tracheids [18]. Its development begins with cells division in the cambium, and then newly formed cells after

several more divisions undergo differentiation through stages of expansion and secondary wall deposition, culminating in mature tracheids apoptosis [19–34]. The kinetics of tree rings formation is studied by counting cell numbers in separate zones of a developing ring on dyed cross-sections of periodically collected samples [25–29]. On a temporal scale, these measurements allow the static pattern at a particular moment in the growth season to be translated into a kinetic pattern that can sometimes even be described by analytical functions [25,29–31]. In addition to tree-specific traits (i.e., species, age, and growth energy), cell number kinetics is naturally regulated by habitat environment (wet, dry, cold, etc.) and intra-seasonal climatic fluctuations [19,28,32,33]. Due to the temporal shift in timeframes of subsequent differentiation stages from one cell to the next one [34–36], information about current environmental fluctuations is presumably recorded sequentially in the kinetics of seasonal growth [23,27,37]. All this modifies the overall growth pattern of a tree and is ultimately reflected in the anatomical characteristics of tree rings, including earlywood-to-latewood ratio, intra-annual density fluctuations (IADFs), cell size, and cell wall thickness [27,31,38–42].

Similarly, the development and validation of mechanistic growth models, such as the Vaganov–Shashkin-process-based model (VS-model), is another potentially efficient method of assessing the influence of external factors on the kinetics of tree-ring seasonal growth and formation [10,20,43–46]. The VS-model allows users to use solar radiation, temperatures, and precipitation as input data to simulate the environment-dependent component of tree-ring width (TRW) variation, making it feasible to compare simulated and actual TRW indices [46–52]. Daily data on these three environmental variables are used in the growth block to calculate intra-seasonal dynamics of tree growth rate and to obtain the TRW index as an integral growth rate over all seasons. The following blocks of the model predict the intra-seasonal increase in the cell number per radial file in the tree ring and their sizes based on the seasonal growth rate curve. However, these blocks are currently in the process of modification to improve their fitness to contemporary datasets and theoretical advancements [15,53]. Recently published comparative studies have revealed a satisfactory convergence between actual measurements of seasonal increase in cell number and their VS-model estimates in several regions [8–10]. The problem of many process models is determining an adequate parameterization approach, which is largely influenced by the number of parameters. The technique of parameterization for the external conditions block of the VS-model, VS-Oscilloscope, has been worked out and sufficiently automated [8,45,54]. It allows users to adapt model performance to various species and habitats. In addition, physiological limits of change for several parameters also facilitate their selection.

In this study, we compared the seasonal kinetics of the cell numbers for five seasons at various stages of differentiation with the calculated growth rate obtained in the VS-model in order to estimate quantitatively close relationships between these direct and simulated indicators of seasonal growth kinetics, and to consider the prospects for using the VS-model as a proxy for direct measurements of the cell number kinetics in different zones of the developing tree ring.

2. Materials and Methods

2.1. Study Area and Sampling Sites

The study was carried out in moisture deficit habitats of the Khakass-Minusinsk Depression, a vast inter-mountain valley in the basin of the Yenisei River (Figure 1). This region experiences a sharply continental climate and receives an annual precipitation of about 350 mm based on the data obtained from Minusinsk weather station (53°41′ N 91°40′ E, 250 m a.s.l., 1936–2021, https://meteo.ru, accessed on 29 September 2022). The sampling was carried out from two different locations during five seasons:

1. An isolated pine forest in the steppe zone near the Minusinsk city (MIN; 2014 and 2017—53°39′ N 91°36′ E, 320 m a.s.l.; 2021—53°40′ N 91°42′ E, 260 m a.s.l.);

2. The forest-steppe ecotone in the foothills of the Batenevsky Range of the Kuznetsk Alatau bordering the valley area near the village of Vershino-Bidzha (BID; 2018–2019—54°00′ N 90°59′ E, 600-650 m a.s.l.).

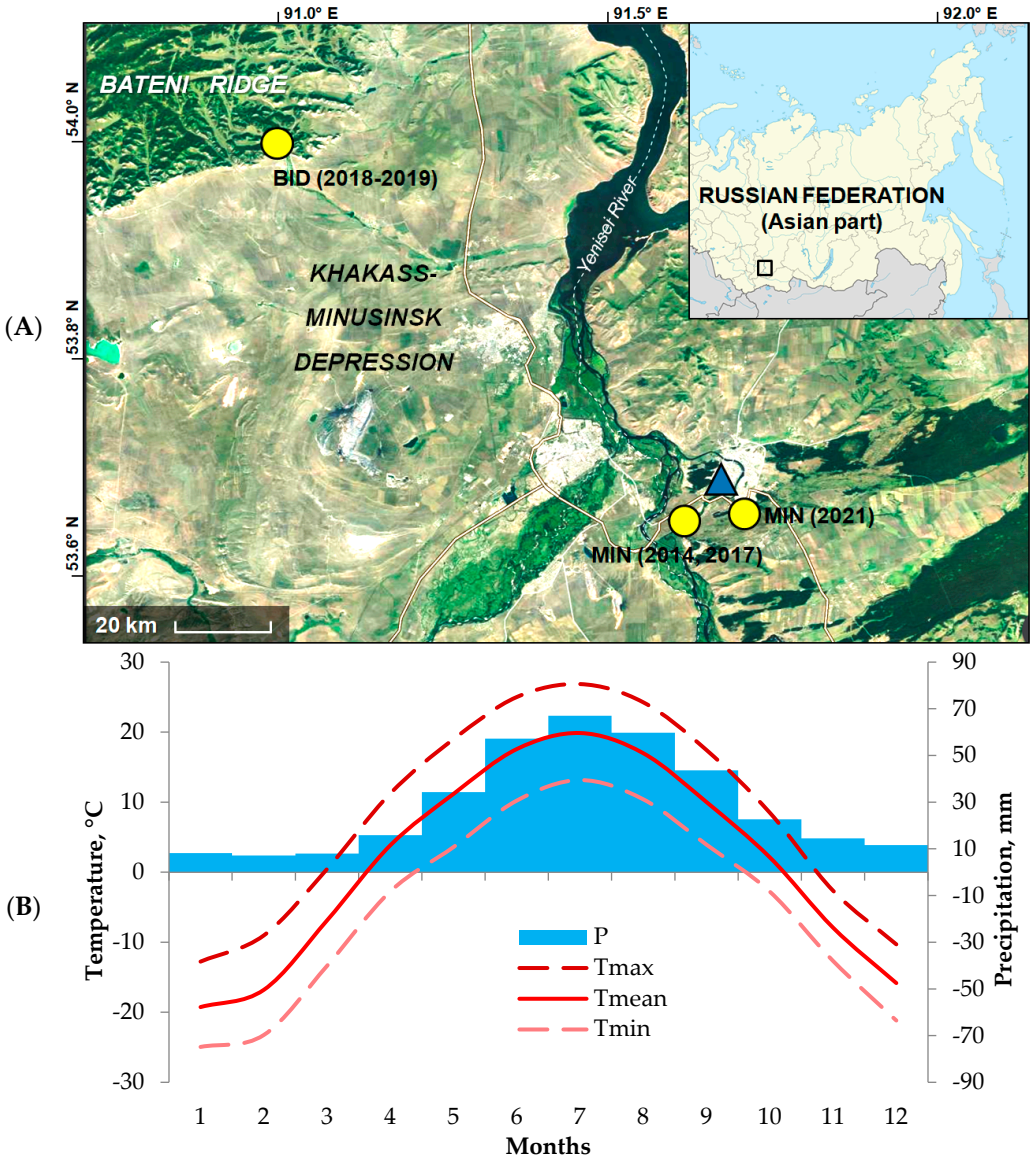

Figure 1. The study area: (**A**) satellite map (© Google) with marked locations of sampling sites (circles) and Minusinsk weather station (triangle); years of sampling are shown next to sampling site codes BID and MIN; inset schematic map (adapted from the Map of Khakassia within Russia (CC BY-SA 4.0) demonstrates the location of the study area (rectangle) in the Asian part of Russia; (**B**) climatic diagram of Minusinsk station (1936–2021): monthly precipitation (P, bars), maximum (Tmax, dark dashed line), mean (Tmean, solid line), and minimum (Tmin, light dashed line) temperatures.

In the steppe zone, forest stands are represented by *Pinus sylvestris* L. trees of different ages on sandy aeolian soils with predominantly flat terrain. The undergrowth bushes cover about 30% of the stand area and comprise *Caragana arborescens* Lam., *Cotoneaster melanocarpus* Fisch. ex Blytt. and *Rosa acicularis* Lindl., while the herbaceous cover (40%–50% of the area) is primarily made up of *Iris ruthenica* Ker.-Gawl., *Phleum phleoides* (L.) H. Karst., *Poa pratensis* L., *Pulsatilla flavescens* (Zucc.) Juz. and *Thalictrum minus* L. Due to their proximity and similarity in terrain, soil, and undergrowth vegetation, the two locations chosen for sampling were assumed to have similar climatic conditions.

The forest-steppe ecotone is signified by a mixed forest stand (*Betula pendula* Roth., *Larix sibirica* Ledeb. and *Pinus sylvestris* L.) on stony loamy soil. Sampling was performed on gentle slopes facing southeast. The forest-steppe ecotone has an undergrowth cover (20%–30%) comprised of *Caragana arborescens* Lam., *Cotoneaster melanocarpus* Fisch. ex Blytt., *Pentaphylloides fruticosa* L., *Spiraea chamaedrifolia* L. and *Rosa acicularis* Lindl, whereas the herbaceous cover (30%–40%) is mainly formed by the *Bupleurum* spp., *Scabiosa ochroleuca* L., *Achillea millefolium* L., *Allium* spp., *Sanguisorba officinalis* L., *Calamagrostis* spp., etc. Moss cover was found to be absent at all sites.

In this study, daily climatic series of the closest Minusinsk weather station (1936–2021) and latitude of each sampling site were used. Despite the substantial distance of Minusinsk station from Vershino-Bidja, its air temperature and precipitation series were found to be more appropriate for dendroclimatic analysis at the BID site compared to Shira, the other available station located at a similar distance; this could be attributed to the flatter terrain between Minusinsk and Vershino-Bidja [55].

2.2. Dendrochronological Data

To study the long-term dynamics of *P. sylvestris* radial growth, wood cores at each site were collected at breast height using an increment borer from more than 20 healthy mature dominant and subdominant trees, which were free of close neighbors and mechanical damage. The full sample at each site (Table 1) included cores from previous expeditions from 2012 to 2017, as well as cores collected at the end of the respective seasons from trees observed for seasonal kinetics. Cores were collected and prepared using standard dendrochronological methods [56]. Tree-ring width (TRW) was measured with an accuracy of 0.01 mm using the LINTAB 5 measuring tool and the TSAPwin program (Rinntech, Germany; [57]). The accuracy of cross-dating of individual TRW series with master chronology was verified using the COFECHA program [58]. Raw measurement series were indexed by eliminating age-related trends described with negative exponent functions, and the TRW index was calculated as the ratio of the actual value to age trend value. The autocorrelation component was then also removed. The individual residual series for each sample site were averaged with a bi-weighted mean to produce the local indexed TRW chronology. The ARSTAN program [59] was used for indexing and generalization.

Table 1. Statistical characteristics of tree-ring width chronologies.

Characteristics	MIN	BID
	Sample	
Number of cores	144	31
Cover period, years	1881–2021	1849–2018
Length, years	141	170
	Residual chronology	
Standard deviation	0.25	0.29
Inter-series correlation coefficient	0.45	0.55
Mean sensitivity	0.30	0.36

2.3. Vaganov–Shashkin Model

To simulate pine growth, VS-model parameters were estimated using local TRW chronologies [20,34,46,60]. The model assumes that three key environmental variables influence seasonal radial growth, including solar radiation, air temperature, and moisture availability (Figure 2). These three factors determine the daily rate of new xylem cells production (growth rate) using the principle of limiting factors. Piecewise linear trapezoidal functions, which approximate the bell-shaped curve of the law of optimum, were used to describe the dependences of the growth rate on soil moisture (estimated using temperature, precipitation, evapotranspiration, and drainage losses) and air temperature. Soil moisture daily changes in the VS-model are defined with the water balance equation, where the dependence of evapotranspiration on temperature is described with an exponential func-

tion [20] (pp. 212); thus, the issue of collinearity does not appear between temperature and soil moisture, or between respective partial growth rates. The partial growth rate due to solar radiation is estimated using latitude and daylength for each calendar date. The general growth rate is then determined by multiplying the partial growth rate caused by solar radiation to the minimal one of partial growth rates related to temperature and water. The onset of the growth season is determined by a specific threshold sum of temperatures for the previous short period, which is usually 60 degree-days over 10 days (Table 7.2 in [20]; cf., critical temperatures 5–8 °C required for xylogenesis described by Rossi et al. [35]). However, the end of the season is not determined in the model other than the temperature partial growth rate being zero for temperatures below minimal for growth. A more detailed description of the growth rate calculation is presented in [20] (pp. 211–214).

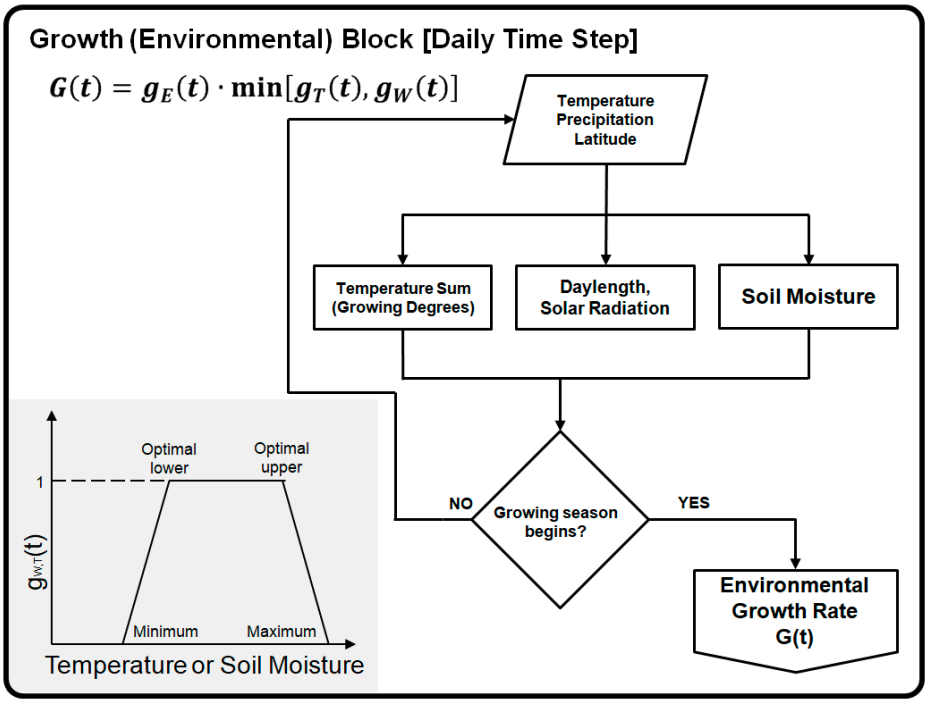

Figure 2. Vaganov–Shashkin model, growth block. Daily growth rates due to the environment are determined by comparing daily temperature and soil moisture (calculated from temperature, precipitation, evapotranspiration, and soil drainage) to piecewise linear approximations of parabolic growth functions (inset). Partial growth rates caused by temperature $g_T(t)$, by soil wetness $g_W(t)$, and by solar radiation estimated from daylength $g_E(t)$ are combined to calculate general growth rate $G(t)$. Figure adapted from Vaganov et al. [34] with permission from Springer Nature.

In addition to climatic series and latitude, the model includes input parameters describing tree species characteristics and habitat conditions (Table 7.2 in [20]). The parameterization (search for the best combination of model constant parameters) was performed using the previously developed and widely tested VS-Oscilloscope tool [54]. The quality of the simulation was examined by dividing the common period of climatic series and TRW chronologies into sub-periods used for calibration and verification. The correlation coefficient *R* and the synchronicity coefficient (*Glk*, the ratio of inter-annual changes unidirectional in two time series [61]) for the simulated and measured TRW indexes, as well as the root mean standard error (*RMSE* [62]), were used as the main indicators of model quality.

2.4. Observations of Seasonal Tree-Ring Development

Seasonal growth kinetics was measured directly by annually selecting 7–10 trees of *P. sylvestris* in the same general area and following the same principles as the sample collected previously for radial growth analysis. Samples were collected from mid-April to mid-September by taking mini cores of 2–3 growth rings on average in every 10-day interval. Sampling was performed using a hand-made instrument similar to Trephor [63] but of a larger diameter (4 mm). Samples were collected at an approximate height of 1.3 m on the southern half of the tree trunk surface in oblique rows 5 cm apart from each other. Collected mini cores were immediately placed in the water-ethanol-glycerol (1:1:1) solution and stored at a temperature of about 6 °C. Wood mini cores were converted into cross-sections of 14–16 µm thickness using a rotary microtome Microm HM 340E (Thermo Fisher Scientific, Waltham, MA, USA). Cross-sections were dyed with safranin and astra blue pigments to distinguish lignified (magenta) tissue from non-lignified (blue) tissue. Microphotographs of cross-sections were taken at 200× magnification using the digital camera ProgRes Gryphax Subra (Jenoptik GmbH, Leipzig, Germany) mounted on the biological microscope BX43 (Olympus, Japan). In each microphotograph, cell numbers were counted and averaged from 5 radial files in the zones of (1) cambium division, (2) cell enlargement, and (3) cell wall thickening and mature tracheids (Figure 3). Cambium cells are the smallest and have the weakest cell walls, resulting in deformed shapes in mounted cross-sections. In the absence of available polarized light images, which are commonly used to determine zone boundaries, we interpreted the color change in radial cell walls from blue to magenta as a sign of lignification and the loss of ability to expand, and such cells were counted as having transited into the cell wall thickening zone. In all images, the end of the radial file was clearly visible at the boundary of the previous ring. To estimate the variability in cell numbers, we calculated the standard error (*SE*) of their mean values for these 5 radial files.

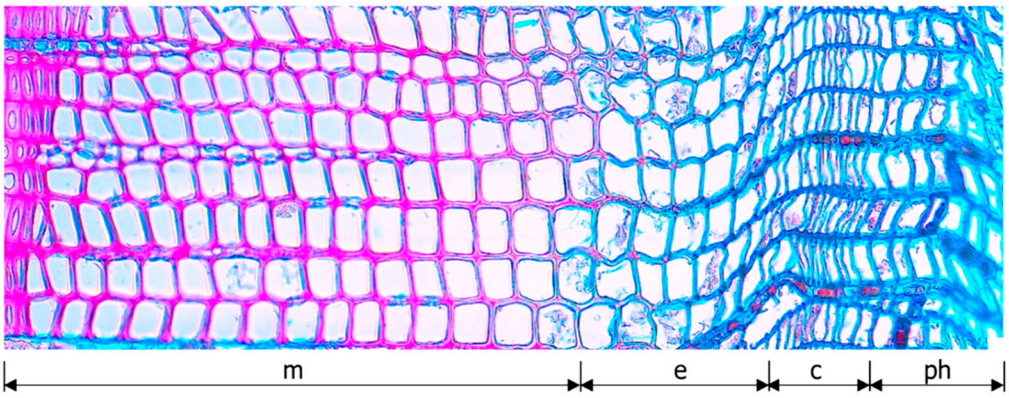

Figure 3. Cross-section of the developing ring of Scots pine sampled on 22 July 2019, at the BID site. Zones are marked as: **ph**, phloem; **c**, cambial zone; **e**, cell enlargement zone; **m**, maturation (wall thickening) and mature cells.

3. Results

3.1. Seasonal Kinetics of Cell Number in the Developing Tree Ring

The number of cells in the cambial zone increased at the beginning of the season, reached a maximum, and then declined back to a minimum (Figure 4). Simultaneously, seasonal characteristics were manifested in the beginning dates of the increase in cambial cell number (e.g., sharp increase from mid-April in 2014), as well as the course of seasonal dynamics (e.g., a second smaller peak in the cambial cell number in 2017). Under prevailing environmental conditions, the highest number of cambial cells in a season were recorded in June and the beginning of July. Although there was a slight delay in the kinetics time of the number of cells in the enlargement zone compared to the cambium cells, the shape replicated the kinetics of the cambial cell number (Figure 4). In comparison to the

enlargement zone, the maturation zone witnessed an additional 15–20 day delay in cell appearance. This delay indicates the time interval required for the first earlywood cells to reach their final size when intense lignification begins. The observed estimates show agreement with results obtained in previous conifer seasonal growth studies performed under various environmental conditions [10,28,31,32,64].

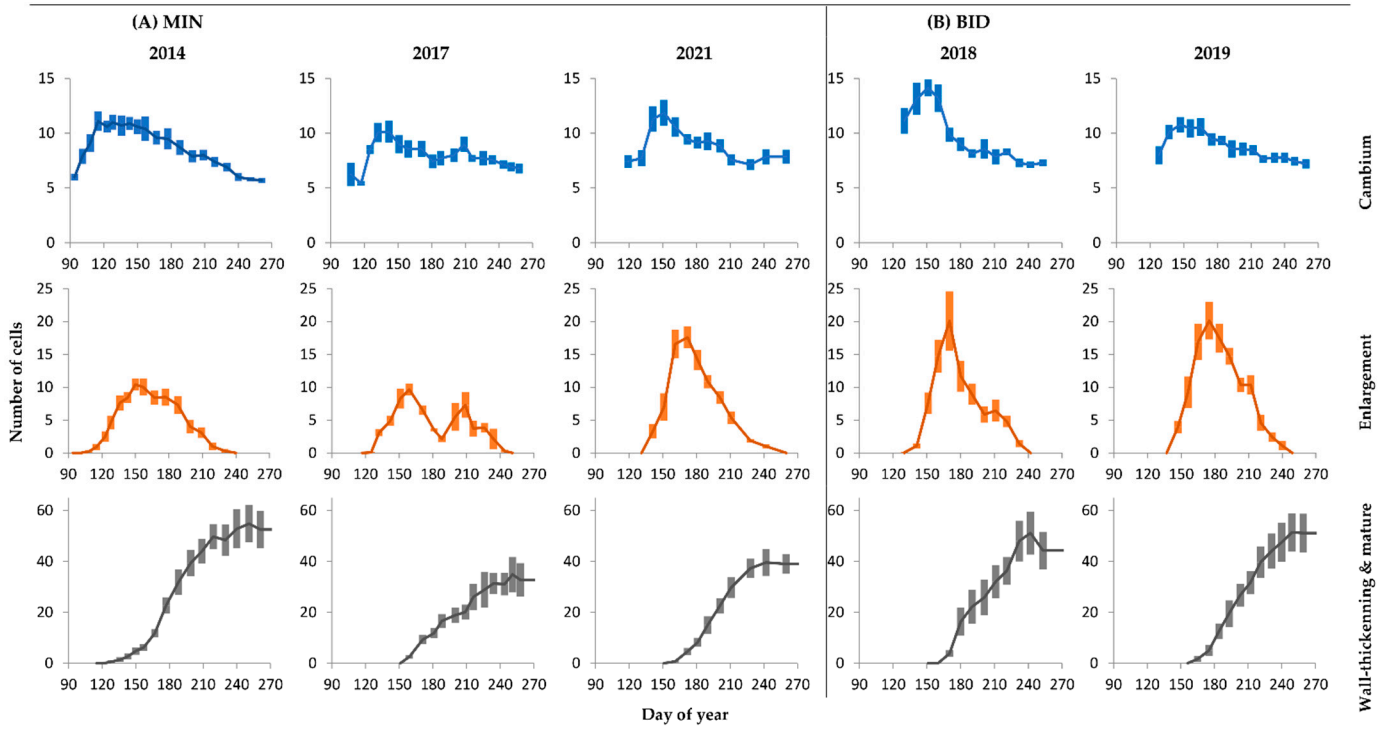

Figure 4. Seasonal kinetics of cell number (mean ± SE) in cambium, cell enlargement zone, and wall-thickening and mature cells in developing tree rings of Scots pine at MIN (**A**) and BID (**B**) sampling sites.

3.2. Simulation of Radial Growth and Calculation of Seasonal Growth Rates

The tree ring chronologies corresponding to the years of seasonal tree ring measurements at each site (2014, 2017, and 2021 at MIN; 2018 and 2019 at BID) were obtained and used for modeling. The main statistical characteristics of the chronologies are summarized in Table 1. The chronologies had similar lengths, standard deviations, and inter-series correlation values.

The values of the parameters of the environmental block of the VS-model selected to ensure the maximum convergence of the simulated and actual growth indices in the VS-Oscilloscope are listed in Table 2, and respective TRW chronologies are presented in Figure 5. The main statistical characteristics showed a significant agreement between the simulated and actual radial growth dynamics at both sites, but the values of these characteristics were slightly higher at the MIN site. Separation of the overlapping period of instrumental climate series and actual chronologies demonstrated the stability of the model fitness with selected parameter values.

The main habitat-related input parameters of the VS-model had different values for each site. Minusinsk exhibited higher optimal and minimum values of soil moisture, whereas Vershino–Bidzha demonstrated higher values of parameters describing evapotranspiration and moisture loss from the soil. This difference is well illustrated by the calculated VS-model soil moisture for the investigated seasons, which was higher at the MIN than at the BID site (Appendix A, Figure A1). The optimal range and maximum temperatures for pine growth were the same at both locations, but the minimum temperature varied by 2 °C.

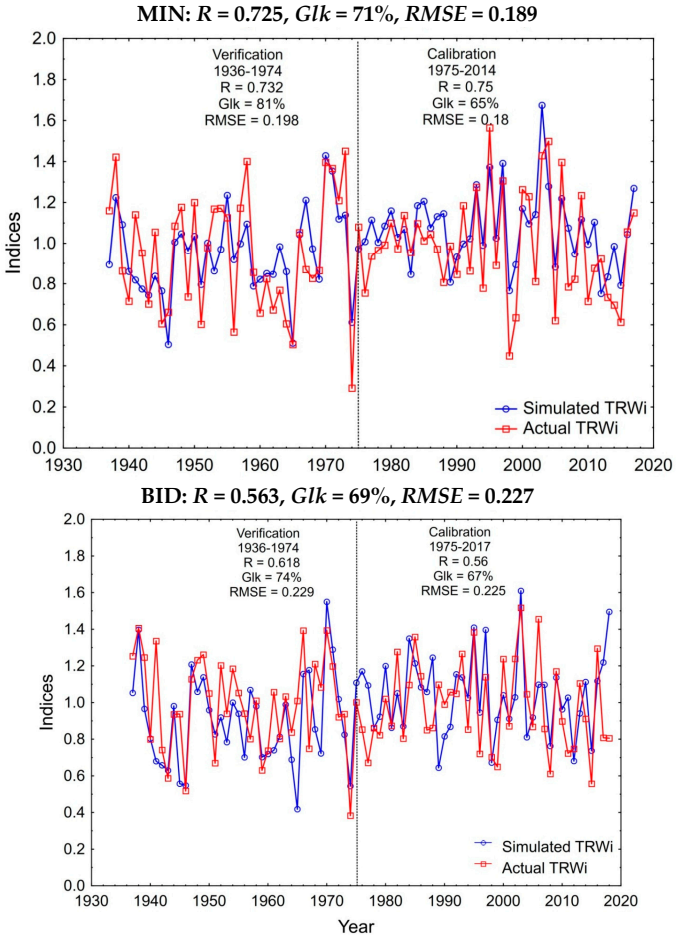

Figure 5. Simulated VS-model (blue) and actual (red) indices of the Scots pine tree-ring width (TRW). Vertical dotted lines divide analysis period into sub-periods of calibration and verification. Presented are statistical characteristics of fitness for entire common period (above plot) and for calibration/verification periods: *R*, correlation between modeled and actual TRW index; *Glk*, synchronicity coefficient; *RMSE*, root-mean-standard error (see Methods).

Table 2. Optimal parameters for growth block in VS-model.

Parameter	Description	MIN	BID
T_{min}	Minimum temperature for tree growth (°C)	7	5
T_{opt1}	Lower end of range of optimal temperatures (°C)	11	11
T_{opt2}	Upper end of range of optimal temperatures (°C)	22	22
T_{max}	Maximum temperature for tree growth (°C)	26	26
W_{min}	Minimum volumetric soil moisture for tree growth, relative to saturated soil (rel. unit)	0.095	0.065
W_{opt1}	Lower end of range of optimal soil moistures (rel. unit)	0.35	0.20
W_{opt2}	Upper end of range of optimal soil moistures (rel. unit)	0.425	0.400
W_{max}	Maximum soil moisture for tree growth (rel. unit)	0.575	0.675
T_{beg}	Temperature sum for initiation of growth (°C)	70	78
l_r	Depth of root system (mm)	500	600
P_{max}	Maximum daily precipitation for saturated soil (mm/day)	42	40
C_1	Fraction of precipitation penetrating soil (not caught by crown; rel. unit)	0.53	0.50
C_2	First coefficient for calculation of transpiration * (mm/day)	0.155	0.258
C_3	Second coefficient for calculation of transpiration * (rel. unit per °C)	0.115	0.165

* In the VS-model, the evapotranspiration is calculated from the daily growth rate from previous day Gr and temperature T with a simplified equation: $C_2 \cdot Gr \cdot \exp(C_3 \cdot T)$.

According to temperature series and calculated soil moisture dynamics (Appendix A, Figure A1), cool temperatures slowed the growth onset in 2014, and moderately low soil moisture was observed throughout the growth season. In 2017, a bout of high temperatures was observed around DOY 170–180, followed by a cool period immediately afterward and steady soil moisture relatively close to optimal. The highest soil moisture for the MIN site across all considered seasons was observed in 2021, accompanied by low temperatures, particularly before DOY 190. At the BID site, after the cool and wet beginning of the season, soil moisture steadily decreased and then stayed low during DOY 170–220 in 2018, while the next season was cooler and slightly less dry, with a drop of soil moisture in the same dates.

Growth rates curves for these seasons (Figure 6) reflected particular features of these seasons, such as drought suppression of growth in both years at the BID site, short-term reaction to hot and dry weather in 2017, and late growth onset in 2021 at the MIN site.

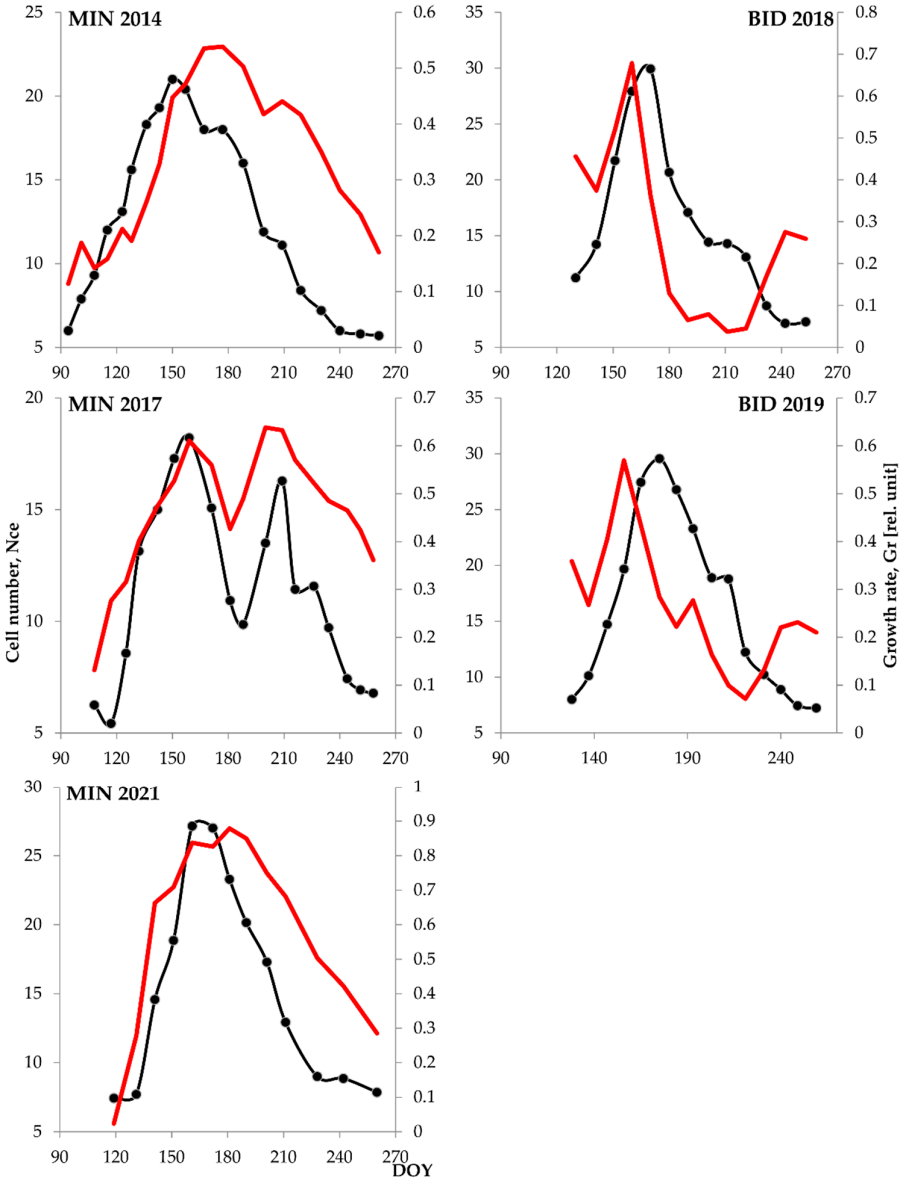

Figure 6. Seasonal kinetics of total cell number in cambial and cell enlargement zones (Nce, black line with markers) and of modeled tree growth rate (Gr, red line) smoothed by 15-day moving average. Horizontal axis represents calendar dates (day of year, DOY) for sampling and for the last day of averaging period of the growth rate.

3.3. Relationship between Observed and Estimated Seasonal Growth Kinetics

Initially, the total cell numbers in the cambium (cell production) and enlargement zones were compared with the daily growth rates obtained in the VS-model on the sampling days. Positive correlations were observed between these two curves. For 2014 and 2021 seasons, correlations were significant at $p < 0.05$ (0.48 and 0.87), while nonsignificant correlations ranged from 0.02 to 0.28 during other seasons. As the simulated growth rates for each season can have significant fluctuations in daily time resolution, the growth rate curves were smoothed using a 15-day moving average to obtain more accurate relationships. The selected 15-day time interval showed correspondence with the estimates of the average duration of the cell enlargement stage for individual tracheids [19,65–68]. Thus, after smoothing, the number of dividing and expanding cells on a certain day was compared with the average growth rate over a 15-day period ending on the same day.

For smoothed growth rate curves, a correlation of 0.56–0.87 (MIN) and 0.26–0.44 (BID) was observed between the simulated growth rate and seasonal kinetics of cell numbers in the cambial and enlargement zones (Figure 6). The shapes of actual and simulated growth rate curves showed notable similarity upon visual examination. According to the graphs, lower correlations at BID were due to the delays between the growth curves. Therefore, cross-correlations between calculated and observed curves reached the maximum values of 0.78 in 2018 and 0.89 in 2019 when the calculated curves were shifted forward by 17 and 20 days, respectively.

On the other hand, the sum of cell numbers in cell expansion, wall thickening zones, and mature tracheids should closely follow the cumulative curve of xylem cells production and, thus, be comparable to the cumulative growth rate curve. However, as both functions are cumulative, likely similar to the Gompertz function due to the general bell-shape of the growth rate and cell production [25], comparison of their stepwise increments should be more informative. In fact, the difference in cumulative growth rate between consecutive sampling dates (or just the sum of daily growth rates) was easily comparable to the difference in the number of differentiating and mature tracheids during the same time interval (Appendix A, Figure A2). In addition to BID in 2018 ($r = 0.16$), all correlations between the curves of growth rate and cell number differences were significant at $p < 0.05$ and ranged from 0.63 to 0.75. However, there was the issue of negative cell number differences calculated sometimes in the second half of the vegetative season.

3.4. Relation between Maximum Cambial Cell Number and Seasonal Production of Tracheids

The maximum number of cambial cells for individual trees was observed between 147 and 193 calendar days of the year (27 May to 12 July). At the same time, the number of cells in the zones of cell wall thickening and mature tracheids was stable after the 240th day of the year (28 August), and from that point until the end of the season (last sampling in the second half of September), the majority of trees completely lacked cells at the stage of enlargement. For each tree, the number of cambial cells during active cell division and the total number of cells in the tree ring were estimated by averaging over these two intra-seasonal intervals. A comparison of the obtained estimates showed positive correlations for all years, and significant linear relationships were found in 2014, 2017, and 2019, as well as in total local and regional datasets (Table 3, Figure 7). At the same time, the linear function always crossed the horizontal axis at a point with a positive number of cambial cells: 1.71–5.60 cells for individual seasons and 3.46–4.24 cells after generalization on the local scale. Local dataset functions were similar to one another and to the generalized function for all observations at both sites, where an axis intercept (the number of cells in the cambium in the absence of production) of 3.59 cells was observed.

Table 3. Dependences of final cell number in tree ring (Ntr) on maximal number of cambial cells (Nc): for individual years, for sampling sites, and for total sample. Linear regressions calculated according to equation Ntr = a·(Nc–Nc_0), where a is the numerical coefficient, and Nc_0 is the number of cambial cells when Ntr = 0.

Sample	Sample Depth	Equation	R^2	p
MIN 2014	10	Ntr = 8.15·(Nc−3.21)	0.75	0.001
MIN 2017	7	Ntr = 6.52·(Nc−3.22)	0.62	0.035
MIN 2021	7	Ntr = 4.71·(Nc−1.71)	0.40	0.125
MIN all years	24	Ntr = 7.28·(Nc−3.46)	0.60	<0.001
BID 2018	7	Ntr = 5.69·(Nc−2.51)	0.12	0.445
BID 2019	9	Ntr = 11.56·(Nc−5.60)	0.61	0.012
BID all years	16	Ntr = 8.03·(Nc−4.24)	0.32	0.023
Total	40	Ntr = 7.36·(Nc−3.59)	0.49	<0.001

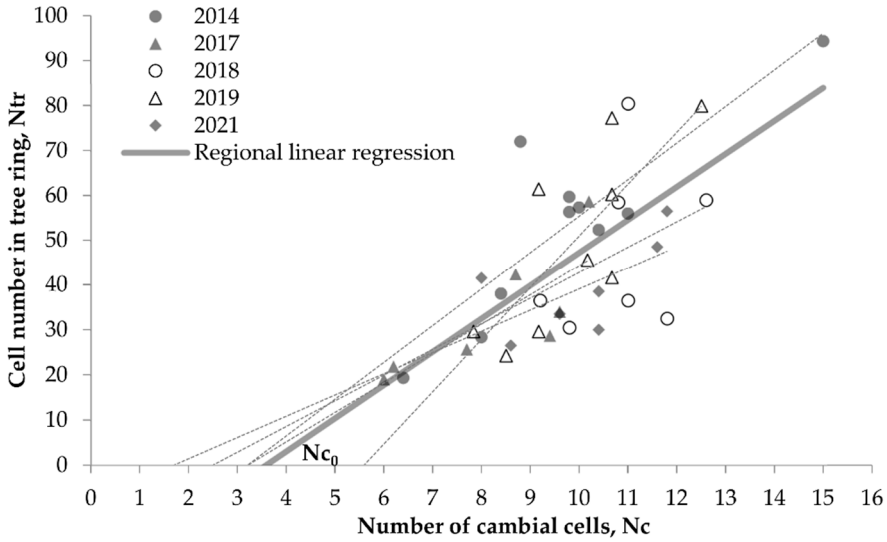

Figure 7. Dependence of final cell number in the tree ring (Ntr) on number of cambial cells (Nc) during the most active part of vegetative season (27 May–12 July). Markers represent individual trees observed at MIN (filled) and BID (empty) sampling sites; lines represent linear regressions for total dataset from two sites (bold solid line) and for particular seasons (thin dotted lines). Nc_0 is number of cambial cells when Ntr = 0.

4. Discussion

4.1. Process-Based Tree Growth Simulation Model and Its Application in the Studied Conditions

The results of this study confirmed the ability of the VS-model to reconstruct tree radial growth dynamics. In the past, the model has produced reliable results not only for the study area [39,50] but also for other moisture-deficient regions [43,47,49,64,69]. Several factors may contribute to the limitations of the model fit to actual data. First, climatic extremes can not only suppress growth processes but also damage tissues, thus having a disproportionately large impact on tree growth [70,71]. This argument was supported by better model values fit for the years of fast and moderate tree growth, but underestimated growth suppression for the years of minimal growth (Figure 5). Second, the VS-model represents the bell-like curve of the law of tolerance with a simplified piecewise linear function, which may lead to biases in the estimations of respective partial growth rates. Third, threshold temperatures are reported to be symmetrical (approximately equal) for the onset of xylogenesis and ending of tracheid differentiation [26,35]. This implies that cambial activity (and TRW formation) terminates at higher temperatures, which is not currently reflected by the VS-model algorithm.

The closer model-to-actual-pine-growth data convergence at the MIN sampling site was probably provided by the proximity of the site to the base weather station. The magnitude of distance between the base weather station and the Minusinsk sites (2–6 km) is much shorter than that of the BID site (58 km), which is mainly responsible for the greater similarity between the climate series of the weather station and actual weather conditions inside the forest stand. This spatial heterogeneity in climatic conditions is particularly more pronounced in the distribution of daily rainfall and consequently, the soil moisture dynamics, and evapotranspiration. The selected values of the main VS-model parameters also reflected the differences in soil conditions. For instance, the higher soil moisture required for pine growth in the Minusinsk forest can be associated with sandy soil, in contrast to the stony and clayey soil in the foothills. The coefficients describing transpiration and moisture loss from the soil disclosed a higher intensity of these processes at the BID site, which was associated with the location of model pine trees on a well-lit southern slope, having a lesser forest-stand canopy cover density, and, consequently, increased soil warming by direct insolation. Additionally, the pine in the Minusinsk forest was able to draw some moisture from deeper soil layers due to the flat terrain and proximity to a watercourse, whereas the slope location of the forest stands at the BID site prevented this from happening. Conifer growth can be influenced not only by air temperature, but also by soil warming at the start of the vegetative season [55,72]. As higher direct surface insolation and faster snowmelt on the sunlit slope can enhance soil warming in spring in the BID site, thawing of the root-inhabited soil layer at lower air temperature can possibly explain the lower minimum air temperature for tree growth obtained by VS-model parameterization for this site despite other temperature boundaries being identical. For the study area with a high continental climate, the maximum threshold of mean daily air temperature of 26 °C corresponds to maximum diurnal temperatures of around 36 °C, putting it in the correct temperature range for suppression of pine growth. Similar maximum temperature threshold values for conifer growth have previously been reported for the VS-model, for example, by Buttò et al. [9].

A comparison of climatic conditions of the studied years (Appendix A, Figure A1) with calculated growth rates suggests that the seasonality of xylogenesis (the timing of the beginning and end of growth) in the study area was primarily regulated by threshold temperatures. However, the rate of xylogenesis was controlled by the water deficit during the majority of the vegetative season. The maximum of cambial activity, in full accordance with the basic equation of the growth rate in VS-model, falls near the summer solstice (21 June), although deviations from it occur due to external stresses during this period. This is consistent with direct observations of seasonal kinetics in this study, which showed that the maximum number of dividing cells occurs within three weeks before and after this date and, thus, supports the idea of photoperiod regulation of xylogenesis [19,73–75].

4.2. Relation between Calculated Growth Rate and Seasonal Kinetics of Xylogenesis

This study has provided the daily dynamics of growth rate to weather conditions as a significant outcome of pine radial growth simulation. As the tree-ring width has a close linear relationship with tracheid production in the cambial zone [20,40,76], intra-seasonal curves of the calculated growth rate can be interpreted as an indirect estimate of the cambial activity kinetics. Indeed, the intra-seasonal curves of calculated growth in the study area showed high similarity to the total cell number curve in the cambial and enlargement zones, which is also supported by the previous observations [45].

Of course, these variables are not equivalent. Their difference and relationship can be comprehended through analogy with water flow in hydrological objects. The number of cells at the early stages corresponds to the water level, whereas inflow represents cell division (i.e., growth rate), and outflow represents the transition of cells into further differentiation stages. Inflow and outflow are balanced in the long term; water level, despite its different nature, is closely related to both and can be calculated.

Following the same principles, the cell number curve in the cambial and cell enlargement zones can be interpreted as an estimate of the xylem cell production rate, assuming (1) a delay for the partial and/or total duration of the cell enlargement stage for individual tracheids, (2) the presence of several cells in the cambial zone during plant dormancy, and (3) the outermost cells of the cambial zone being dedicated to phloem production. For the considered trees, the number of cambial cells during dormancy was relatively stable. Phloem cell production exhibits a correlation with xylem cell production, but higher stability and less susceptibility to environmental factors [77,78]. It has been reflected by a closer linear relationship between the rate of total cell production in the cambial zone and the number of xylem cells versus phloem cells [77]. Moreover, both indicators were several times lower than xylem production for the relatively wide tree rings considered in this study. Therefore, in the first approximation, the curve of total cell number in the cambial and enlargement zones can be described as a linear transformation of the curve of actual xylem cell production, taking into account the delay for a period from the last mother cell division up to the end of cell expansion, i.e., up to 20 days and more [19,65–68].

As a result, the close similarity in the shape of curves (both visual and linear regression) for the simulated growth rate from the VS-model and the actually observed kinetics of cell number in the early stages of xylogenesis supports the predominant contribution of the cell division rate to the result of xylogenesis and the high convergence of the model with actually occurring growth processes at the cell scale.

4.3. Dependence of Seasonal Tracheid Production on the Maximum Cell Number in the Cambial Zone

It should be noted that the relationship between the total production of xylem cells per season and the maximum number of dividing cells in the cambial zone was positive at both sites and for all considered vegetative seasons. As the rate of xylem cell production within trees appears to vary between different radii [79–81], the technique used to collect wood samples from varying radii during the season is thought to be the primary source of uncertainty. The small sample size (number of trees) for each season also contributed to the high variability of the numerical coefficients and the low significance level of the correlations. As a result, when samples from different seasons are combined, both within-site and on a regional scale, the empirical dependence became more stable and gained a higher level of significance. Based on the timeframe of direct observations of these related variables, we can conclude that the obtained function can be used for short-term forecasting of the seasonal production of Scots pine xylem cells in the study area from the number of cambial cells near the summer solstice. Such a prediction can be helpful in forest management operations because the tree-ring width and its dependent indicators of tree productivity (e.g., basal area increment BAI) are closely related to the seasonal production of xylem cells [20,40,76]. The pattern of quantitative coefficients for this relationship is also interesting: for all considered individual seasons, and generalized local and regional datasets, this linear dependence crosses the horizontal axis at a positive number of cambial cells, the range of which is limited. As the independent variable is the maximum intra-seasonal value for cambial cell number, this allows us to hypothesize that for pine in the study area, even under the most extreme conditions and at complete rest, the cambial zone contains at least three or four cells (theoretically, the cambium initial cell, one-two xylem mother cells, and one phloem mother cell).

5. Conclusions

We studied the seasonal dynamics in tree-ring development of Scots pine from moisture-deficit habitats of the Khakass-Minusinsk Depression. The simulated VS-model daily growth rate, based on soil moisture and air temperature, showed notable accordance with actually observed new xylem cell production dynamics. The highest number of cambial cells in a season, recorded near the summer solstice, demonstrated a positive

relationship with the final total number of tracheids in the tree ring, projecting this variable as a promising short-term predicting estimation for tree radial growth and productivity.

Author Contributions: Conceptualization, E.A.V.; methodology, E.A.V. and E.A.B.; validation, L.V.B. and K.K.U.; formal analysis, G.A.S., G.K.Z. and L.V.B.; investigation, D.F.Z. and E.A.B.; resources, L.V.B. and D.F.Z.; data curation, L.V.B.; writing—original draft preparation, L.V.B., E.A.V., D.F.Z. and E.A.B.; writing—review and editing, L.V.B., D.F.Z. and K.K.U.; visualization, G.A.S., G.K.Z. and L.V.B.; supervision, E.A.V.; project administration, D.F.Z.; funding acquisition, E.A.V. and E.A.B. All authors have read and agreed to the published version of the manuscript.

Funding: This study was funded by the Russian Foundation for Basic Research, grant number 20-016-00049 (direct observations of seasonal tree-ring formation); by the Russian Science Foundation, grant number 19-18-00145 (simulation of tree growth).

Data Availability Statement: The data presented in this study are available on request from the corresponding author.

Acknowledgments: The authors are grateful to Ivan I. Tychkov (Siberian Federal University) for performing calculations in VS-Oscilloscope program, results of which are presented in Figure 5 and Table 2.

Conflicts of Interest: The authors declare no conflict of interest. The funders had no role in the design of the study; in the collection, analyses, or interpretation of data; in the writing of the manuscript, or in the decision to publish the results.

Appendix A

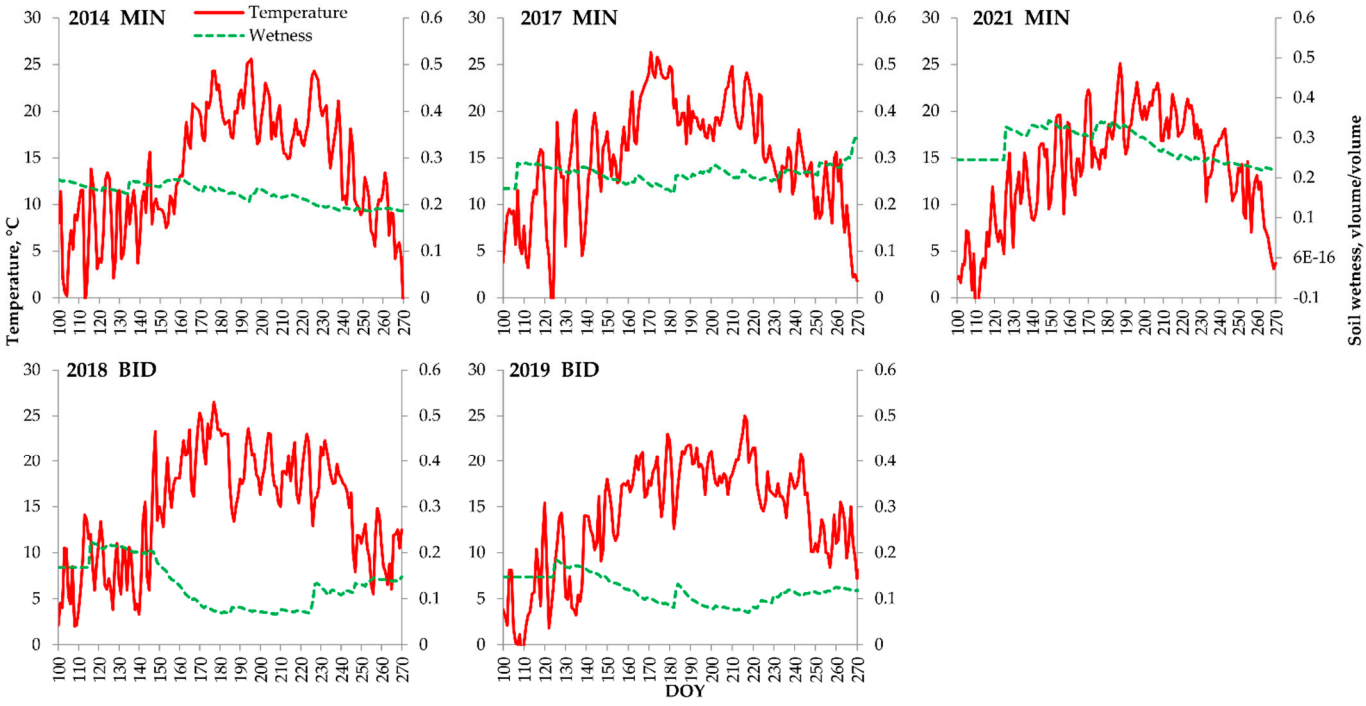

Figure A1. Climatic characteristics of years when growth seasonal kinetics observations were carried out: daily mean air temperature (red solid line) and calculated VS-model soil wetness (green dashed line; calculated only during active vegetation). Climatic series are from Minusinsk station.

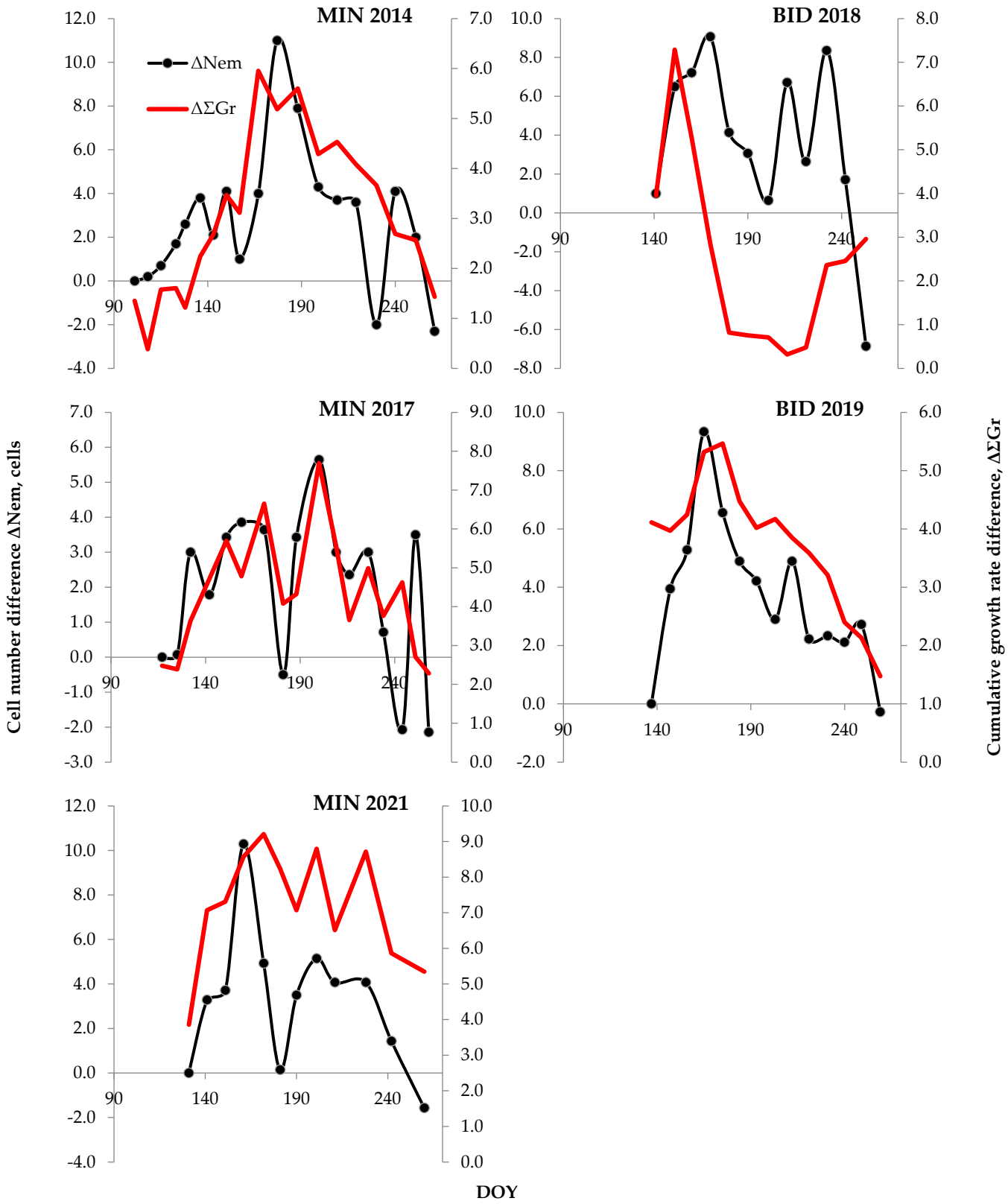

Figure A2. Seasonal kinetics of differences in total cell number in cell enlargement, wall-thickening, and mature zones (ΔNem, black line with markers), and of modeled cumulative tree growth rate (ΔΣGr, red line); each point is the difference between dates of current and previous sampling. The horizontal axis represents calendar dates (day of year, DOY) for current sampling.

References

1. Meinhardt, H. *Models of Biological Pattern Formation*; Academic Press: London, UK, 1982; p. 211.
2. Bessonov, N.; Volpert, V. *Dynamical Models of Plant Growth*; Publibook: Paris, France, 2006; p. 63.
3. Peng, C. Understanding the role of forest simulation models in sustainable forest management. *Environ. Impact Assess. Rev.* **2000**, *20*, 481–501. [CrossRef]
4. Prusinkiewicz, P.; Runions, A. Computational model of plant development and form. *New Phytol.* **2012**, *193*, 549–569. [CrossRef] [PubMed]
5. Lazareva, G.G.; Mironova, V.V.; Omelyanchuk, N.A.; Shvab, I.V.; Vshivkov, V.A.; Gorpinchenko, D.N.; Nikolaev, S.V.; Kolchanov, N.A. Mathematical modeling of plant morphogenesis. *Numer. Anal. Appl.* **2008**, *1*, 123–134. [CrossRef]
6. Guiot, J.; Boucher, E.; Gea-Izquierdo, G. Process models and model-data fusion in dendroecology. *Front. Ecol. Evol.* **2014**, *2*, 52. [CrossRef]
7. Fonti, M.V.; Fakhrutdinova, V.V.; Kalinina, E.V.; Tychkov, I.I.; Popkova, M.I.; Shishov, V.V.; Nikolaev, A.N. Long-term variability of anatomic features of annual tree rings of larch, pine and spruce in the permafrost zone in central Siberia. *Contemp. Probl. Ecol.* **2019**, *12*, 692–702. [CrossRef]
8. Fonti, M.V.; Tychkov, I.I.; Churakova (Sidorova), O.V. Intra-seasonal climatic signal in tree ring of conifers in the permafrost zone of Siberia. *Russ. J. Ecol.* **2021**, *52*, 412–418. [CrossRef]
9. Butto, V.; Shishov, V.; Tychkov, I.; Popkova, M.; He, M.; Rossi, S.; Deslaurier, A.; Morin, H. Comparing of cell dynamics of tree ring formation observed in microcores and as predicted by the Vaganov-Shashkin model. *Front. Plant Sci.* **2020**, *11*, 1268. [CrossRef]
10. Tumajer, J.; Kaspar, J.; Kuzelova, H.; Shishov, V.; Tychkov, I.; Popkova, M.I.; Vaganov, E.A.; Treml, V. Forward modeling reveals multidecadal trends in cambial kinetics and phenology at treeline. *Front. Plant Sci.* **2021**, *12*, 613643. [CrossRef]
11. Kramer, E.M. A mathematical model of auxin-mediated radial growth of trees. *J. Theor. Biol.* **2001**, *208*, 387–397. [CrossRef]
12. Jonsson, H.; Heisler, M.G.; Shapiro, B.E.; Meyerowitz, E.M.; Mjolsness, E. An auxin-driven polarized transport model for phyllotaxis. *Proc. Natl. Acad. Sci. USA* **2006**, *103*, 1633–1638. [CrossRef]
13. Hay Mele, B.; Giannino, F.; Vincenot, C.E.; Mazzoleni, E.; Carteni, F. Cell-based models of plant developmental biology: Insights into hybrid approaches. *Front. Environ. Sci.* **2015**, *3*, 73. [CrossRef]
14. Hartmann, F.P.; Rathgeber, C.B.K.; Fournier, M.; Moulia, B. Modelling wood formation and structure: Power and limits of a morphogenetic gradient in controlling xylem cell proliferation and growth. *Ann. For. Sci.* **2017**, *74*, 14. [CrossRef]
15. Belousova, D.A.; Shishov, V.V.; Babushkina, E.A.; Vaganov, E.A. VS-Cambium-developer: A new approach to modeling the functioning of the cambial zone of conifers under the influence of environmental factors. *Russ. J. Ecol.* **2021**, *52*, 358–367. [CrossRef]
16. Chiatante, D.; Montagnoli, A.; Trupiano, D.; Sferra, G.; Bryant, J.; Rost, T.L.; Scippa, G.S. Meristematic connectome: A cellular coordinator of plant responses to environmental signals? *Cells* **2021**, *10*, 2544. [CrossRef]
17. Hartmann, F.P.; Rathgeber, C.B.; Badel, E.; Fournier, M.; Moulia, B. Modelling the spatial crosstalk between two biochemical signals explains wood formation dynamics and tree-ring structure. *J. Exp. Bot.* **2021**, *72*, 1727–1737. [CrossRef]
18. Schweingruber, F.H. *Microscopic Wood Anatomy: Structural Variability of Stems and Twigs in Recent and Subfossil Woods from Central Europe*; WSL: Birmensdorf, Switzerland, 1990; p. 226.
19. Rathgeber, C.B.K.; Pérez-de-Lis, G.; Fernández-de-Uña, L.; Fonti, P.; Rossi, S.; Treydte, K.; Gessler, A.; Deslauriers, A.; Fonti, M.V.; Ponton, S. Anatomical, developmental and physiological bases of tree-ring formation in relation to environmental factors. In *Stable Isotopes in Tree Rings*; Siegwolf, R.T.W., Renée Brooks, J., Roden, J., Saurer, M., Eds.; Springer: Cham, Germany, 2022; pp. 61–99. [CrossRef]
20. Vaganov, E.A.; Hughes, M.K.; Shashkin, A.V. *Growth Dynamics of Conifer Tree Rings: Images of Past and Future Environments*; Springer: Berlin, Germany, 2006; p. 358.
21. Larson, P.R. *The Vascular Cambium. Development and Structure*; Springer: Berlin, Germany, 1994; p. 725.
22. Cartenì, F.; Deslauriers, A.; Rossi, S.; Morin, H.; De Micco, V.; Mazzoleni, S.; Giannino, F. The physiological mechanisms behind the earlywood-to-latewood transition: A process-based modeling approach. *Front. Plant Sci.* **2018**, *9*, 1053. [CrossRef]
23. Rossi, S.; Deslauriers, A.; Anfodillo, T. Assessment of cambial activity and xylogenesis by microsampling tree species: An example at the Alpine timberline. *IAWA J.* **2006**, *27*, 383–394. [CrossRef]
24. Rathgeber, C.B.; Cuny, H.E.; Fonti, P. Biological basis of tree-ring formation: A crash course. *Front. Plant Sci.* **2016**, *7*, 734. [CrossRef]
25. Rossi, S.; Deslaurier, A.; Morin, H. Application of the Gompertz equation for the study of xylem cell development. *Dendrochronologia* **2003**, *21*, 33–39. [CrossRef]
26. Li, X.; Liang, E.; Gricar, J.; Rossi, S.; Cufar, K.; Ellison, A.M. Critical minimum temperature limits xylogenesis and maintains treeline on the southeastern Tibetan Plateau. *Sci. Bull.* **2017**, *62*, 804–812. [CrossRef]
27. Vaganov, E.A.; Babushkina, E.A.; Belokopytova, L.V.; Zhirnova, D.F. Small fluctuations in cell wall thickness in pine and spruce: Signal from cambium? *PLoS ONE* **2020**, *15*, e0233106. [CrossRef] [PubMed]
28. Fonti, M.V.; Babushkina, E.A.; Zhirnova, D.F.; Vaganov, E.A. Xylogenesis of Scots pine in an uneven-aged stand of the Minusinsk Depression (Southern Siberia). *J. Sib. Fed. Univ. Biol.* **2020**, *13*, 197–207. [CrossRef]
29. He, M.; Yang, B.; Wang, Z.; Bräuning, A.; Pourtahmasi, K.; Oladi, R. Climatic forcing of xylem formation in Qilian juniper on the northeastern Tibetan Plateau. *Trees* **2016**, *30*, 923–933. [CrossRef]

30. Huang, J.-G.; Deslaurier, A.; Rossi, S. Xylem formation can be modeled statistically as a function of primary growth and cambium activity. *New Phytol.* **2014**, *203*, 831–841. [CrossRef] [PubMed]
31. Yu, B.; Li, X.; Zhao, P.; Huang, J. Comparison of intra-annual xylem and phloem formation of *Picea crassifolia* stands at two latitudes in Northwest China. *Forests* **2021**, *12*, 1445. [CrossRef]
32. Peters, R.L.; Steppe, K.; Cuny, H.E.; De Pauw, D.J.W.; Frank, D.C.; Schaub, M.; Rathgeber, C.B.K.; Cabon, A.; Fonti, P. Turgor – a limiting factor for radial growth in mature conifers along an elevational gradient. *New Phytol.* **2021**, *229*, 213–229. [CrossRef]
33. Pompa-García, M.; Hevia, A.; Camarero, J.J. Minimum and maximum wood density as proxies of water availability in two Mexican pine species coexisting in a seasonally dry area. *Trees* **2021**, *35*, 597–607. [CrossRef]
34. Vaganov, E.A.; Anchukaitis, K.J.; Evans, M.N. How well understood are the processes that create dendroclimatic records? A mechanistic model of the climatic control on conifer tree-ring growth dynamics. In *Dendroclimatology: Progress and Prospects*; Hughes, M.K., Swetnam, T.W., Diaz, H.F., Eds.; Springer: Dordrecht, Germany, 2011; pp. 37–75. [CrossRef]
35. Rossi, S.; Deslauriers, A.; Griçar, J.; Seo, J.W.; Rathgeber, C.B.; Anfodillo, T.; Morin, H.; Levanic, T.; Oven, P.; Jalkanen, R. Critical temperatures for xylogenesis in conifers of cold climates. *Glob. Ecol. Biogeogr.* **2008**, *17*, 696–707. [CrossRef]
36. Olano, J.M.; Eugenio, M.; Garcia-Cervigon, A.I.; Folch, M.; Rozas, V. Quantitative tracheid anatomy reveals a complex environmental control of wood structure in continental Mediterranean climate. *Int. J. Plant Sci.* **2012**, *173*, 137–149. [CrossRef]
37. Eilmann, B.; Zweifel, R.; Buchmann, N.; Graf Pannatier, E.; Rigling, A. Drought alters timing, quantity, and quality of wood formation in Scots pine. *J. Exp. Bot.* **2011**, *62*, 2763–2771. [CrossRef]
38. Pacheco, A.; Camarero, J.J.; Ribas, M.; Gazol, A.; Gutierrez, E.; Carrer, M. Disentangling the climate-driven bimodal growth pattern in coastal and continental Mediterranean pine stands. *Sci. Total Environ.* **2018**, *615*, 1518–1526. [CrossRef]
39. Popkova, M.; Vaganov, E.A.; Shishov, V.V.; Babushkina, E.A.; Rossi, S.; Bryukhanova, M.V.; Fonti, P. Modeled tracheidograms disclose drought influence on *Pinus sylvestris* tree-rings structure from Siberian forest-steppe. *Front. Plant Sci.* **2018**, *9*, 1144. [CrossRef]
40. Babushkina, E.A.; Belokopytova, L.V.; Zhirnova, D.F.; Vaganov, E.A. Siberian spruce tree ring anatomy: Imprint of developmental processes and their high-temporal environmental regulation. *Dendrochronologia* **2019**, *53*, 114–124. [CrossRef]
41. Gao, J.; Rossi, S.; Yang, B. Origin of intra-annual density fluctuations in a semi-arid area of Northwestern China. *Front. Plant Sci.* **2021**, *12*, 777753. [CrossRef]
42. Palla, B.; Ladányi, M.; Cseke, K.; Buczkó, K.; Höhn, M. Wood anatomical traits reveal different structure of peat bog and lowland populations of *Pinus sylvestris* L. in the Carpathian region. *Forests* **2021**, *12*, 494. [CrossRef]
43. Yang, B.; He, M.; Shishov, V.; Tychkov, I.; Vaganov, E.; Rossi, S.; Ljungqvist, F.C.; Bräuning, A.; Grießinger, J. New perspective on spring vegetation phenology and global climate change based on Tibetan Plateau tree-ring data. *Proc. Natl. Acad. Sci. USA* **2017**, *114*, 6966–6971. [CrossRef]
44. Shishov, V.V.; Tychkov, I.I.; Popkova, M.I.; He, M.; Yang, B.; Rozenberg, P. Global tree-ring growth evolution neural network (VS-GENN). *Le Stud. Multidiscip. J.* **2018**, *2*, 9–20. [CrossRef]
45. Tychkov, I.I.; Sviderskaya, I.V.; Babushkina, E.A.; Popkova, M.I.; Vaganov, E.A.; Shishov, V.V. How can the parameterization of a process-based model help us understand real tree-ring growth? *Trees* **2019**, *33*, 345–357. [CrossRef]
46. Anchukaitis, K.J.; Evans, M.N.; Hughes, M.K.; Vaganov, E.A. An interpreted language implementation of the Vaganov-Shashkin tree-ring proxy system model. *Dendrochronologia* **2020**, *60*, 125677. [CrossRef]
47. Touchan, R.; Shishov, V.V.; Meko, D.M.; Nouiri, I.; Grachev, A. Process based model shed light on climate sensitivity of Mediterranean tree-ring width. *Biogeosciences* **2012**, *9*, 965–972. [CrossRef]
48. Breitenmoser, P.; Bronnimann, S.; Frank, D. Forward modeling of tree-ring width and comparison with a global network of tree-ring chronologies. *Clim. Past* **2014**, *10*, 437–449. [CrossRef]
49. Zhang, J.; Gou, X.; Zhang, Y.; Lu, M.; Xu, X.; Zhang, F.; Liu, W.; Gao, L. Forward modeling analysis of Qilian Juniper (*Sabina przewalskii*) growth in response to climate factors in different regions of the Qilian Mountains, northwestern China. *Trees* **2016**, *30*, 175–188. [CrossRef]
50. Babushkina, E.A.; Zhirnova, D.F.; Belokopytova, L.V.; Tychkov, I.I.; Vaganov, E.A.; Krutovsky, K.V. Response of four species to changing climate in a moisture-limited area of South Siberia. *Forests* **2019**, *10*, 999. [CrossRef]
51. Wu, M.; Liu, N.; Bao, G.; Gao, J. Climatic factors of radial growth of *Pinus tabulaeformis* in eastern Gansu, Northwest China based on Vaganov-Shashkin model. *Geogr. Ann. Ser. A Phys. Geog.* **2020**, *102*, 196–208. [CrossRef]
52. Matskovsky, V.; Venejas-Gonzalez, A.; Garreand, R.; Roig, F.A.; Gutierrez, A.; Minoz, A.A.; LeQuesue, C.; Klock, K.; Canales, C. Tree growth decline as a response to projected climate change in the 21st century in Mediterranean mountain forests of Chile. *Glob. Planet Chang.* **2021**, *198*, 103406. [CrossRef]
53. Shishov, V.V.; Tychkov, I.I.; Anchukaitis, K.J.; Zelenov, G.K.; Vaganov, E.A. A band model of cambium development: Opportunities and prospects. *Forests* **2021**, *12*, 1361. [CrossRef]
54. Shishov, V.V.; Tychkov, I.I.; Popkova, M.I.; Ilyin, V.A.; Bryukhanova, M.V.; Kirdyanov, A.V. VS-Oscilloscope: A new tool to parameterize tree radial growth based on climate conditions. *Dendrochronologia* **2016**, *39*, 42–50. [CrossRef]
55. Belokopytova, L.V.; Zhirnova, D.F.; Meko, D.M.; Babushkina, E.A.; Vaganov, E.A.; Krutovsky, K.V. Tree rings reveal the impact of soil temperature on larch growth in the forest-steppe of Siberia. *Forests* **2021**, *12*, 1765. [CrossRef]
56. Cook, E.R.; Kairiukstis, L.A. *Methods of Dendrochronology: Applications in the Environmental Sciences*; Kluwer Academic Publishers: Dordrecht, The Netherlands, 1990; p. 394.

57. Rinn, F. *TSAP-Win: Time Series Analysis and Presentation for Dendrochronology and Related Applications: User Reference*; RINNTECH: Heidelberg, Germany, 2003.
58. Holmes, R.L. Computer-assisted quality control in tree-ring dating and measurement. *Tree-Ring Bull.* **1983**, *43*, 68–78.
59. Cook, E.R.; Krusic, P.J. *Program ARSTAN: A Tree-Ring Standardization Program Based on Detrending and Autoregressive Time Series Modeling, with Interactive Graphics*; Lamont-Doherty Earth Observatory, Columbia University: Palisades, NY, USA, 2005.
60. Anchukaitis, K.J.; Evans, M.N.; Kaplan, A.; Vaganov, E.A.; Hughes, M.K.; Grissino-Mayer, H.D.; Cane, M.A. Forward modeling of regional scale tree-ring patterns in the southeastern United States and the recent influence of summer drought. *Geophys. Res. Lett.* **2006**, *33*, L04705:1–L04705:4. [CrossRef]
61. Buras, A.; Wilmking, M. Correcting the calculation of Gleichläufigkeit. *Dendrochronologia* **2015**, *34*, 29–30. [CrossRef]
62. Russell, M.B.; Weiskittel, A.R.; Kershaw, J.A., Jr. Assessing model performance in forecasting long-term individual tree diameter versus basal area increment for the primary Acadian tree species. *Can. J. For. Res.* **2011**, *41*, 2267–2275. [CrossRef]
63. Rossi, S.; Anfodillo, T.; Menardi, R. Trephor: A new tool for sampling microcores from tree stems. *IAWA J.* **2006**, *27*, 89–97. [CrossRef]
64. He, M.; Yang, B.; Shishov, V.; Rossi, S.; Bräuning, A.; Ljungqvist, F.C.; Grießinger, J. Relationships between wood formation and cambium phenology on the Tibetan Plateau during 1960–2014. *Forests* **2018**, *9*, 86. [CrossRef]
65. Wodzicki, T.J. Mechanism of xylem differentiation in *Pinus sylvestris* L. *J. Exp. Bot.* **1971**, *22*, 670–687. [CrossRef]
66. Skene, D.S. The kinetics of tracheid development in *Tsuga canadensis* Carr. and its relation to tree vigour. *Ann. Bot.* **1972**, *36*, 179–187. [CrossRef]
67. Rathgeber, C.B.K.; Longuetaud, F.; Mothe, F.; Cuny, H.; Le Moguédec, G. Phenology of wood formation: Data processing, analysis and visualisation using R (package CAVIAR). *Dendrochronologia* **2011**, *29*, 139–149. [CrossRef]
68. Cuny, H.E.; Rathgeber, C.B.K.; Frank, D.; Fonti, P.; Fournier, M. Kinetics of tracheid development explain conifer tree-ring structure. *New Phytol.* **2014**, *203*, 1231–1241. [CrossRef]
69. He, M.; Shishov, V.; Kaparova, N.; Yang, B.; Brauning, A.; Griessinger, J. Process-based modeling of tree-ring formation and its relationships with climate on the Tibetan Plateau. *Dendrochronologia* **2017**, *42*, 31–41. [CrossRef]
70. Frank, D.; Reichstein, M.; Bahn, M.; Thonicke, K.; Frank, D.; Mahecha, M.D.; Smith, P.; van der Velde, M.; Vicca, S.; Babst, F.; et al. Effects of climate extremes on the terrestrial carbon cycle: Concepts, processes and potential future impacts. *Glob. Chang. Biol.* **2015**, *21*, 2861–2880. [CrossRef]
71. Shao, H.; Zhang, Y.; Gu, F.; Shi, C.; Miao, N.; Liu, S. Impacts of climate extremes on ecosystem metrics in southwest China. *Sci. Total Environ.* **2021**, *776*, 145979. [CrossRef]
72. Sanmiguel-Vallelado, A.; Camarero, J.J.; Morán-Tejeda, E.; Gazol, A.; Colangelo, M.; Alonso-González, E.; Lopez-Moreno, J.I. Snow dynamics influence tree growth by controlling soil temperature in mountain pine forests. *Agric. For. Meteorol.* **2021**, *296*, 108205. [CrossRef]
73. Asante, D.K.; Yakovlev, I.A.; Fossdal, C.G.; Holefors, A.; Opseth, L.; Olsen, J.E.; Junttila, O.; Johnsen, Ø. Gene expression changes during short day induced terminal bud formation in Norway spruce. *Plant Cell Environ.* **2011**, *34*, 332–346. [CrossRef] [PubMed]
74. Petterle, A.; Karlberg, A.; Bhalerao, R.P. Daylength mediated control of seasonal growth patterns in perennial trees. *Curr. Opin. Plant Biol.* **2013**, *16*, 301–306. [CrossRef] [PubMed]
75. Jyske, T.; Mäkinen, H.; Kalliokoski, T.; Nöjd, P. Intra-annual tracheid production of Norway spruce and Scots pine across a latitudinal gradient in Finland. *Agric. For. Meteorol.* **2014**, *194*, 241–254. [CrossRef]
76. Babushkina, E.A.; Dergunov, D.R.; Belokopytova, L.V.; Zhirnova, D.F.; Upadhyay, K.K.; Tripathi, S.K.; Zharkov, M.S.; Vaganov, E.A. Non-linear response to cell number revealed and eliminated from long-term tracheid measurements of Scots pine in Southern Siberia. *Front. Plant Sci.* **2021**, *12*, 719796. [CrossRef]
77. Gričar, J.; Prislan, P.; Gryc, V.; Vavrčík, H.; De Luis, M.; Čufar, K. Plastic and locally adapted phenology in cambial seasonality and production of xylem and phloem cells in *Picea abies* from temperate environments. *Tree Physiol.* **2014**, *34*, 869–881. [CrossRef]
78. Miller, T.W.; Stangler, D.F.; Larysch, E.; Seifert, T.; Spiecker, H.; Kahle, H.P. Plasticity of seasonal xylem and phloem production of Norway spruce along an elevational gradient. *Trees* **2020**, *34*, 1281–1297. [CrossRef]
79. Kozlowski, T.T.; Winget, C.H. Diurnal and seasonal variation in radii of tree stems. *Ecology* **1964**, *45*, 149–155. [CrossRef]
80. Fritts, H.C. *Tree Rings and Climate*; Academic Press: London, UK, 1976; p. 567.
81. Mäkinen, H.; Vanninen, P. Effect of sample selection on the environmental signal derived from tree-ring series. *For. Ecol. Manag.* **1999**, *113*, 83–89. [CrossRef]